

3D simulations of shear instabilities in magnetized flows

M. Brüggen^{1,2}, W. Hillebrandt¹

¹ Max-Planck-Institut für Astrophysik, Karl-Schwarzschild-Str. 1, 85740 Garching, Germany

² Churchill College, Storey's Way, Cambridge, CB3 0DS, UK

27 October 2018

ABSTRACT

We present results of three-dimensional (3D) simulations of the magnetohydrodynamic Kelvin-Helmholtz instability in a stratified shear layer. The magnetic field is taken to be uniform and parallel to the shear flow. We describe the evolution of the fluid flow and the magnetic field for a range of initial conditions. In particular, we investigate how the mixing rate of the fluid depends on the Richardson number and the magnetic field strength. It was found that the magnetic field can enhance as well as suppress mixing. Moreover, we have performed two-dimensional (2D) simulations and discuss some interesting differences between the 2D and 3D results.

Key words: hydrodynamics, stars

1 INTRODUCTION

Observational evidence seems to suggest that current formalisms underestimate the efficiency of the mixing processes that operate in stars, especially in fast rotating stars. Therewhile, the observational evidence for mixing is increasing rapidly. Herrero et al. (1992) find that all fast rotating O-stars show significant surface He-enrichments. Other observations include the N/C and ¹³C and ¹²C enrichments of stars on the Red Giant Branch (e.g. Kraft et al. 1997, Charbonnel 1995), the He and N excesses in OBA supergiants (Fransson et al. 1989), the depletion of boron in most B-type stars (Venn, Lambert & Lemke 1996) and the ratio of the number of blue to red supergiants in galaxies (Langer & Maeder 1995). For a more detailed review see Maeder (1995), Kraft (1994) and references therein. These observations seem to suggest that mixing is strong enough to transport the nuclearily processed material to the surface in a fraction of the life time of the star. It has been shown that, both, the enrichment in CNO elements and the depletion of fragile elements such as boron can be explained if some form of mixing is introduced (Langer 1992, Denissenkov 1994, Denissenkov & Tout 2000, Meynet & Maeder 1997).

The Kelvin-Helmholtz instability occurs in chemically homogeneous, stratified shear flows when the destabilising effect of the relative motion in the different layers dominates over the stabilising effect of buoyancy (see e.g. Chandrasekhar 1961). The competition between the two effects is described by the Richardson number, Ri :

$$Ri = \frac{g\rho'}{\rho U'^2}, \quad (1)$$

where ρ is density, U the shear velocity and g the gravitational acceleration. The prime indicates the derivative in the direction of gravity. Maeder (1995, 1997) and Maeder & Zahn (1998) generalised the Richardson criterion to include radiative losses and changes in the chemical potential. For a further discussion of the Richardson number the reader is referred to their papers.

Magnetic fields in stars are believed to be produced by differential rotation and are predominantly toroidal (e.g. Parker 1979). In the Sun it is thought that the magnetic field is concentrated at the bottom of the convection zone. The bottom of the convection zone is also the perceived location of the solar dynamo which is believed to be responsible for the solar cycle. Within the convection zone flux expulsion and magnetic buoyancy swiftly remove any toroidal magnetic field.

Seismic measurements of the rotation rate of the Sun have revealed a differentially rotating convection zone and a rigidly rotating interior with a shear layer that separates the two. However, the explanations for the peculiar rotation rates of the Sun remain controversial. The most convincing proposals involve shear-generated quasi-horizontal turbulence (Spiegel & Zahn 1992) or a large-scale magnetic field in the radiative interior (Gough & McIntyre 1998). The differential rotation of the Sun and other stars is only one of the issues that demonstrate the importance of simulating shear instabilities in the presence of magnetic fields. The mag-

netic Kelvin-Helmholtz instability has been treated in other physical contexts, for example in the heliosphere, where the solar wind flows past planetary magnetospheres (see, e.g., Ubertoi 1984), in the context of the stability of interstellar clouds (Vietri, Ferrara & Miniati 1997) and in accretion disks (Anzer & Börner 1983).

Apart from mixing by shear instabilities, there is another important candidate believed to be responsible for extra mixing in stars, namely convective overshoot. This mechanism has been investigated numerically by a number of groups (Freytag, Ludwig & Steffen 1996, Nordlund & Stein 1996, Singh, Roxburgh & Chan 1998) all of which find some degree of overshoot. Observations seem to support this: Isochrone fitting to stellar clusters and binary systems suggests that convective overshoot is significant (see Zahn 1991 for a review).

In this paper we simulate shear instabilities in a stratified magnetized fluid. The magnetic field can change the picture that was obtained in the unmagnetized case (see Brüggen & Hillebrandt 2000) in various ways: The instability can locally enhance or diminish the magnetic field, which, in turn, can enhance dissipation by reconnection and alter the flow pattern.

When the field is parallel to the shear flow, magnetic tension will have a stabilising influence on the flow. This can be regarded as a consequence of the field line tension whose effect is similar to the effect of surface tension, e.g. in Rayleigh-Taylor instabilities. If the field is perpendicular to the direction of the flow, it affects the flow only through an extra pressure which changes the magnetosonic speed. A linear analysis of the magnetohydrodynamic shear instability was presented by Chandrasekhar (1961).

In the incompressible case it can be shown that a uniform magnetic field, that is aligned with the shear flow, stabilises the Kelvin-Helmholtz instability as long as the velocity jump across the shear layer is less than twice the Alfvén speed. For the compressible case, Miura & Pritchett (1982) presented a linear stability analysis, but in order to proceed further, numerical simulations were required.

Malagoli et al. (1996) performed a set of 2D MHD simulations of the KH instability in a uniform magnetic field where they varied the ratio of the Alfvén to the sound speed. They could identify three stages in which the instability develops: the linear stage, the dissipative transient stage with intermittent reconnection events and the saturation stage, where the turbulence decays into aligned structures. These findings were confirmed by Kepvens et al. (1999). These authors reported 2D MHD simulations for the case where the magnetic field was unidirectional everywhere and for the case where the magnetic field changes sign in the middle of the shear layer. The two cases were found to be dynamically very different.

In a series of papers Jeong et al. (2000), Jones et al. (1997) and Frank et al. (1996) presented 2- and 2.5-dimensional simulations of uniform shear layers in the presence of magnetic fields of varying strength and direction. In the non-magnetic case it is known that shear flows develop a vortex, also known as “Cat’s Eye”, which would spin for

a long time before viscous dissipation would eventually dissolve it. In the MHD case, however, the authors cited above find that the quasi-steady state of the flow is a nearly laminar layer instead of a single big vortex. The magnetic tension stabilises the flow before the vortex can form. Instead, a broad shear layer develops. This may not be too surprising for strong magnetic field but it was not obvious that even very weak fields can fundamentally alter the flow. For fields just below the critical field strength the aforementioned authors found that enhancements of the magnetic field through linear growth can stabilise the flow before it becomes nonlinear. Even fields that are by a factor of 2.5 weaker than the critical field strength were found to reconnect and reorganise the flow such as to quickly relax into a marginally stable laminar flow. Even though the magnetic field was initially weak, it was strong enough for magnetic stresses to become important before the formation of the primary vortex.

Very recently, Ryu, Jones & Frank (2000) published results of 3D simulations of the nonlinear evolution of a uniform (unstratified) shear layer. They performed high resolution simulations mainly with the intention to study the turbulent properties of uniform MHD flows. We, on the other hand, did not aim to simulate full MHD turbulence, for which our resolution would be insufficient. Instead, we make a first attempt at quantifying mixing rates in magnetized, compressible and stratified shear flows as a function of the Richardson number. For this purpose we performed a set of 3D and 2D MHD simulations and investigated the dependence of the mixing rate on the Richardson number and the magnetic field strength. Moreover, we studied the nonlinear dynamics of the magnetic shear instability and investigated the differences between 2D and 3D simulations. With conditions in stellar interiors in mind, we restricted ourselves to subsonic flows. As far as we know, to date, these are the first 3D simulations of the magnetohydrodynamic Kelvin-Helmholtz instability in a *stratified* fluid.

2 NUMERICAL SIMULATIONS

Here we present the results of numerical simulations of the magnetohydrodynamic shear instability in a stratified fluid. The simulations were obtained using the ZEUS-3D code which was developed especially for problems in astrophysical hydrodynamics (Clarke & Norman 1994). The code uses finite differencing on a Eulerian or pseudo-Lagrangian grid and is fully explicit in time. It is based on an operator-split scheme with piecewise linear functions for the fundamental variables. The fluid is advected through a mesh using the upwind, monotonic interpolation scheme of van Leer. The magnetic field is evolved using a modified constrained transport technique which ensures that the field remains divergence-free to machine precision. The electromotive forces are computed via upwind differencing along Alfvén characteristics. For a detailed description of the algorithms and their numerical implementation see Stone & Norman (1992a, b).

As initial model, an isothermal density distribution under constant gravitational acceleration in hydrostatic equilibrium was chosen. The initial density distribution is shown in Fig. 1. In the following, we will use dimensionless units

Table 1. Initial parameters of the simulations: ratio of the mean Alfvén velocity, v_A , to the adiabatic sound speed, c_s , and ratios of the mean Alfvén velocities to the velocity jump across the shear layer for $Ri = 0.1, 0.2$ and 0.3 .

	$\frac{v_A}{c_s}$	$\frac{v_A}{\Delta v}$ (0.1)	$\frac{v_A}{\Delta v}$ (0.2)	$\frac{v_A}{\Delta v}$ (0.3)
$B = 0.001$	$2.6 \cdot 10^{-3}$	0.05	0.07	0.09
$B = 0.003$	$7.5 \cdot 10^{-3}$	0.15	0.21	0.27
$B = 0.01$	$2.6 \cdot 10^{-2}$	0.50	0.71	0.91

which are determined by a gravitational constant of $G = 1$, a gravitational acceleration of $g = 0.01$ and a density scale height of 10. Then a shear velocity profile was imposed on the fluid. It was assumed to have the form of a hyperbolic tangens in order to minimise the effect of the boundaries onto the shear layer, i.e.

$$U(z) = U_0 \tanh[(z - z_0)/h], \quad (2)$$

where U_0 is the amplitude of the shear (x -) velocity, z the vertical position of the shear layer, and h its extent. In order to keep the shear layer away from the boundaries, h was taken to be smaller than the vertical extent of the simulation region. U_0 was chosen to yield a range of initial Richardson numbers of $0.05 - 0.3$, where the Richardson number is taken in its original simple definition, i.e. $Ri = g\rho'/\rho U'^2$ and is measured at $z = z_0$. Finally, B was chosen to yield a range of Alfvén velocities which extend up to the velocity jump across the shear layer (see Table 1 and 2 for details). As shown in Table 2, the magnetic energy ranges from $\sim 1\%$ of the kinetic energy to a few times the kinetic energy. In this paper we only consider the case where the initial magnetic field is uniform and parallel to the shear flow (uni-directional everywhere). For comparison, we also repeated the simulations with the magnetic field set to zero. Fig. 1 shows the initial conditions for $Ri = 0.1, 0.2$, and 0.3 . The boundary conditions were chosen to be periodic in the x -direction and reflecting in the y - and z -direction.

In our simulations we employed an ideal gas equation of state, we ignored the effects of rotation, nuclear reactions and radiative processes. The simulations were computed on a Cartesian grid and the computational domain had the dimensions $2 \times 1 \times 1$ (in the x -, y - and z -direction, where gravity acts in the z -direction). It was covered by $100 \times 50 \times 50$ grid points. For comparison, we also performed 2D simulations on a grid with 200×100 grid points. The calculations were performed on a CRAY T3E and an IBM RS/6000 cluster.

In order to study mixing processes, the ZEUS code was modified to follow the motion of 1000 ‘tracer’ particles. They are advected with the fluid and are initially located in a plane perpendicular to the z -axis in the centre of the shear layer.

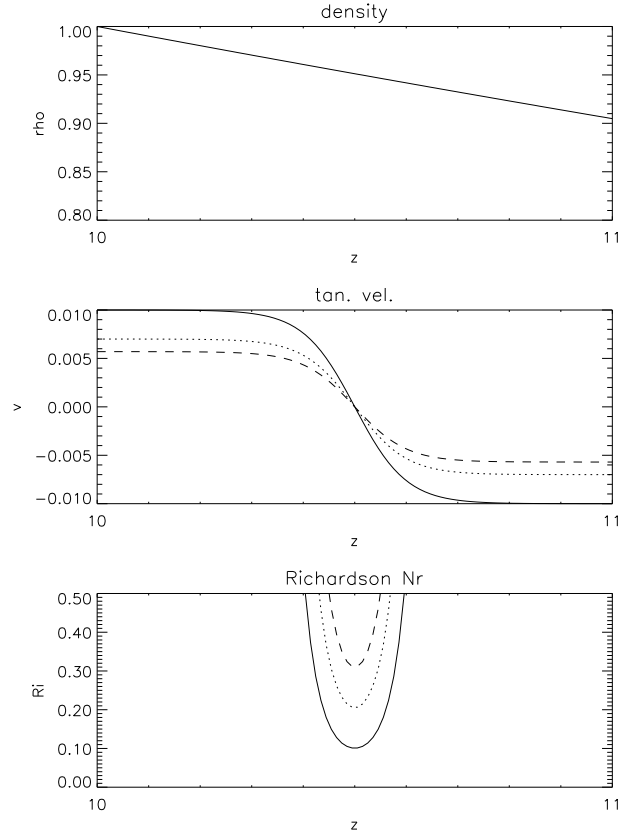


Figure 1. Initial density and shear velocity distributions. The bottom panel shows the Richardson numbers for the respective velocities (correspondence denoted by the same line style).

Table 2. Initial parameters of the simulations: ratio of the initial magnetic energy to the initial kinetic energy for different Richardson numbers.

Ri	0.1	0.15	0.2	0.3
$B = 0.001$	$1.32 \cdot 10^{-2}$	$2.04 \cdot 10^{-2}$	$2.70 \cdot 10^{-2}$	$4.01 \cdot 10^{-2}$
$B = 0.003$	0.118	0.183	0.243	0.360
$B = 0.01$	1.316	2.037	2.699	4.012

3 RESULTS AND DISCUSSION

First, we will briefly present the results of our 2D simulations and discuss how they compare with the previous numerical work that was mentioned in Sec. 1. Then we will compare the 2D simulations with the 3D simulations. In the non-magnetic case (Brüggen & Hillebrandt 2000), we found that the 2D and 3D simulations yielded very similar results for the mixing rates. Here we will investigate whether this is still the case when magnetic fields are involved.

3.1 2D simulations

In general, we found that the effect of the magnetic field on the shear instability is multifarious and diverse: The mag-

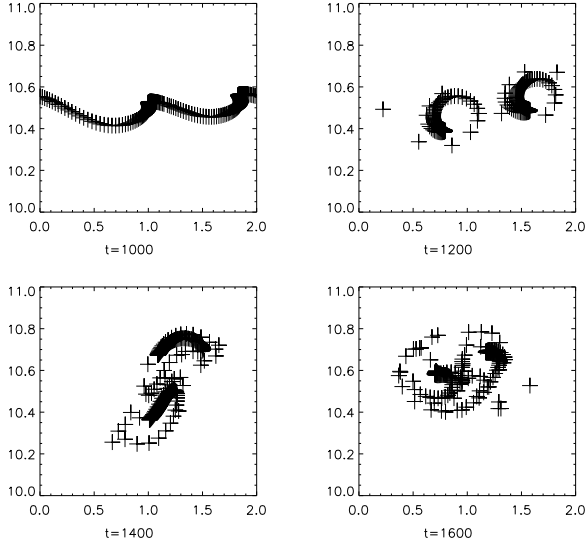


Figure 2. Positions of tracer particles at various times for a 2D simulation with $Ri=0.2$ and no magnetic field.

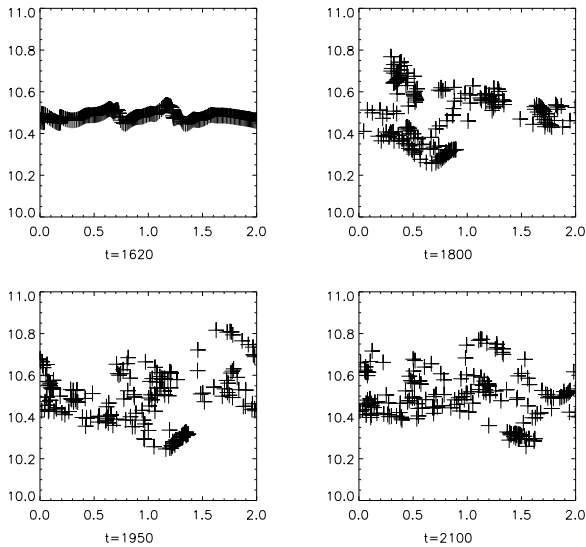


Figure 3. Positions of tracer particles at various times for a 2D simulation with $Ri=0.2$ and $B=0.001$.

netic field can enhance as well as diminish the mixing, depending on the strength of the shear. Fig. 2-4 show the positions of tracer particles at various times in some 2D simulations with a Richardson number of $Ri=0.2$, for magnetic fields of $B = 0$, $B = 0.001$ and $B = 0.003$, respectively. Immediately, one can note that the magnetic field suppresses the formation of the characteristic primary vortex at the centre of the shear layer and inhibits the mixing. Instead of a vortex a broad laminar mixing layer develops. The tracer particles remain within the shear layer and are not swirled around as much as in the case without a magnetic field. This suppression becomes more effective the stronger the magnetic fields is. Stronger magnetic fields lead to a narrower shear layer as the Maxwell stresses tend to align the magnetic and velocity fields. This is also apparent in the

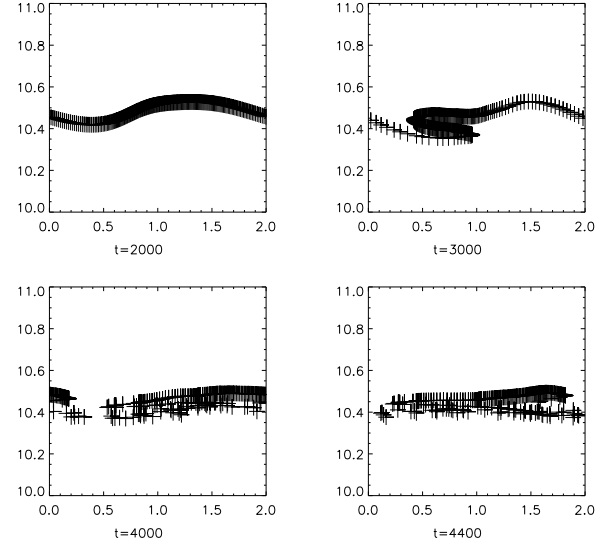


Figure 4. Positions of tracer particles at various times for a 2D simulation with $Ri=0.2$ and $B=0.003$.

transverse (z -) velocities and the vorticity. The maximum z -velocities and vorticities decrease with increasing magnetic field strength. A strong magnetic field tends to stabilize any slight transverse motion before a vortex can form. Relatively weak field are being wound up by the shear flow. During this winding-up the magnetic field strength locally exceeds its initial value by up to a factor of ~ 12 for the $B = 0.001$ and $Ri=0.1$ run. For the runs with a higher Richardson number or higher magnetic fields this enhancement decreases. We should point out that this amplification of the field is not the result of some dynamo action. The local enhancement of the magnetic field comes from the stretching and twisting of the magnetic field lines. As one may have expected, we find that regions of high vorticity and enhanced magnetic fields are correlated.

To visualise the working and evolution of the magnetic field, we show the magnetic energy for two quite different examples. Fig. 5 shows the magnetic energy for a 'weak' field in which the dynamic effect of the magnetic field is relatively small with $Ri=0.1$, $B = 0.001$. A different situation is seen in Fig. 6 which shows the evolution of a 'strong' field with $Ri=0.2$, $B = 0.003$. In the latter case, the magnetic field efficiently reduces the mixing in the shear layer. In Fig. 5 one can see that a big vortex forms, which subsequently decays, while in Fig. 6 the field undulates a little but remains essentially laminar. In both cases the magnetic energy increases with time, and this increase is stronger for the more dynamic case shown in Fig. 5. In the weak field case the magnetic flux is expelled from the centre of the vortex.

For the very strong magnetic field of $B = 0.01$, all shear flows with $Ri \geq 1$ remained stable for well over 3000 sound crossing times where we stopped the simulation.

This behaviour agrees qualitatively with the works of Frank et al. (2000) and Jeong et al. (2000) although their initial conditions somewhat differ from ours. The reader is referred to their paper for further details of the Kelvin-

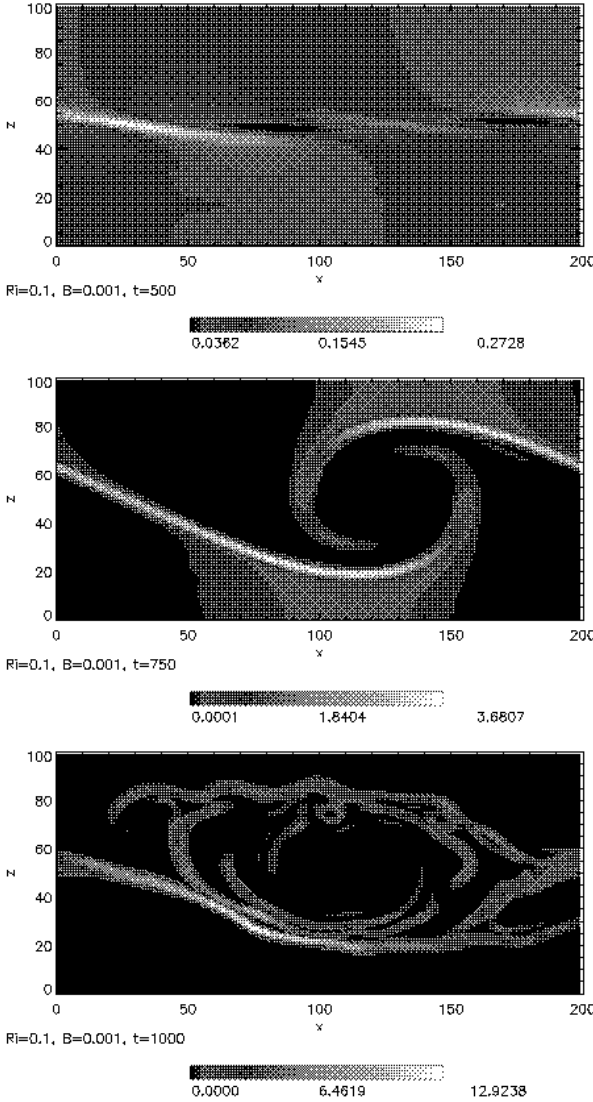


Figure 5. Magnetic energy in a 2D simulation with $Ri=0.1$ and $B = 0.001$.

Helmholtz instability in 2D simulations.

While in the simulations with Richardson numbers > 1 the effect of the magnetic field was to suppress the mixing, we found the effect to be reversed for the case with a low Richardson number and a strong magnetic field ($Ri=0.1$ and $B = 0.003$). Now the magnetic field seems to enhance the mixing. The positions of the tracer particles are shown in Fig. 7 and the magnetic energy is plotted in Fig. 8. Again, one can note that the magnetic field is bundled together in two flux tubes which form at the centre of the shear layer and are aligned with the flow. Subsequently, the flux tubes drift to the edges of the shear layer and, in doing so, mix the fluid. This can be seen in the distribution of the tracer particles in Fig. 7. Eventually, numerical reconnection occurs and the magnetic field forms a filamentary structure in the shear layer.

In Sec. 1, we mentioned the importance of mixing in the context of stellar evolution. For this purpose, it is use-

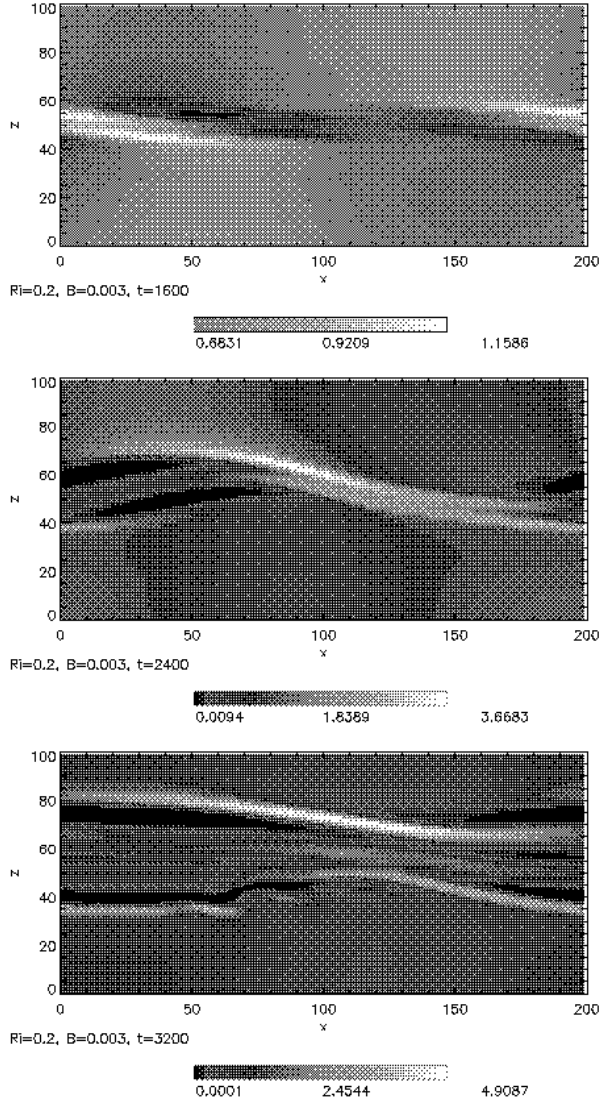


Figure 6. Magnetic energy in a 2D simulation with $Ri=0.2$ and $B = 0.003$.

ful to quantify the rate of mixing by some kind of one-dimensional diffusive approximation, because most stellar evolution codes implement the mixing through a diffusion equation. A heuristic diffusion constant can then be defined as follows (Brüggen & Hillebrandt 2000)

$$D = \sigma^2/t, \quad (3)$$

where $\sigma^2 = \frac{1}{N} \sum_N [z(N) - z_0]^2$, N being the number of tracer particles, z_0 the original height of the tracer particle and z its height after a time t . The diffusion coefficient as a function of time has been plotted in Fig. 9 for one particular example of parameters. As in the non-magnetic case described in Brüggen & Hillebrandt (2000), the diffusion coefficient rises with time before it reaches its maximum. Then it remains approximately constant, apart from some turbulent scatter, before it slowly starts to decrease again. The nearly constant value to which D is converging is the value which is of greatest interest for the purpose of evolving stellar models.

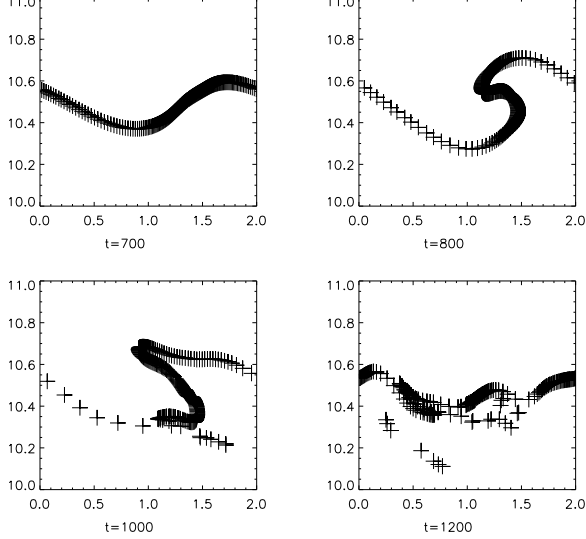


Figure 7. Positions of tracer particles at various times for a 2D simulation with $Ri=0.1$ and $B=0.003$.

In Fig. 10 we show the diffusion constant as a function of the Richardson number for the different magnetic field strengths. The errorbars indicate the residual scatter. Obviously, D decreases with increasing Richardson number similar to the non-magnetic case. But furthermore, the power of the magnetic field to suppress the mixing becomes evident. The diffusion coefficients for the cases with $B = 0.003$ are by a factor of a few smaller than the respective cases with $B = 0.001$ as long as $Ri > 0.1$. For $Ri=0.1$, however, the diffusion coefficient for the strong magnetic field lies above the low field case.

To make the Richardson number the only controlled parameter in our study, constitutes a severe simplification of the factors that determine the efficiency of mixing. In reality, the efficiency of mixing will depend on the density stratification and the velocity gradient separately, and not solely through the Richardson number. Moreover, the mixing will depend on the exact shape of the velocity profile and, only to a first approximation, on its first derivative. Nevertheless, if one has to pick a single parameter to describe the shear flow, e.g. for stellar evolution studies, the Richardson number would be the most suitable one.

3.2 3D simulations

In the 3D simulations for the case with $Ri=0.1$ and $B = 0.001$, we found that the suppression of the primary vortex is less effective than in the 2D simulations. In Fig. 11 we have plotted the positions of the tracer particles for the same case as in Fig. 3, but now taken from the 3D simulations. In the 3D simulations, contrary to the 2D case, a big primary vortex forms which vigorously mixes the tracer particles. This vortex is transitory and decays approximately within one turnover time, as already observed in the unmagnetised case. The final distribution of the tracer particles looks more like the unmagnetized case than the 'laminar' picture in Fig. 3. In 3D the magnetic field does not seem to be able to sup-

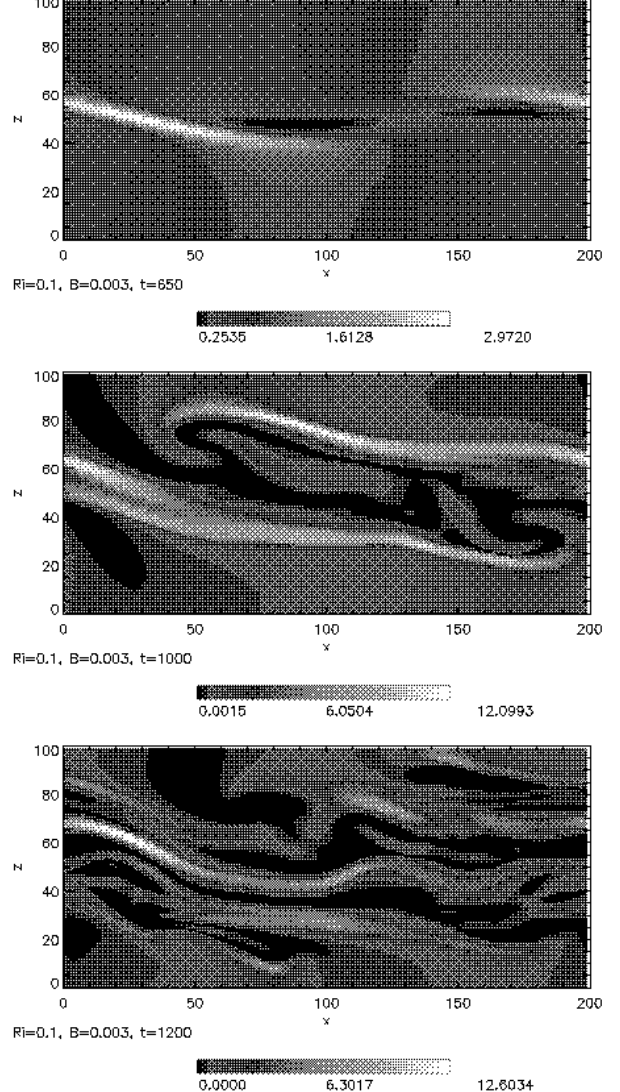


Figure 8. Magnetic energy in a 2D simulation with $Ri=0.1$ and $B = 0.003$.

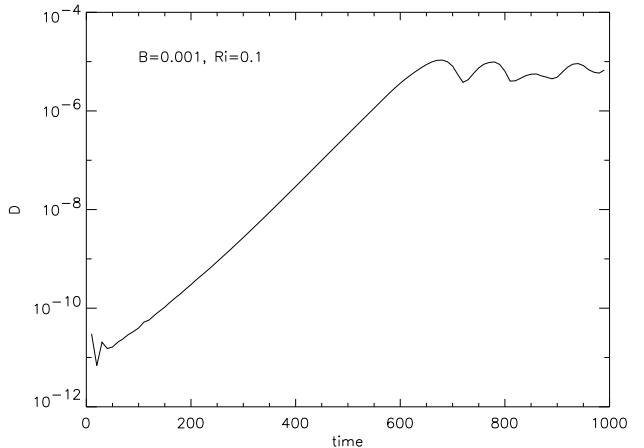


Figure 9. Dimensionless diffusion coefficient as a function of time for $Ri=0.2$ and $B=0.001$ (2D simulation).

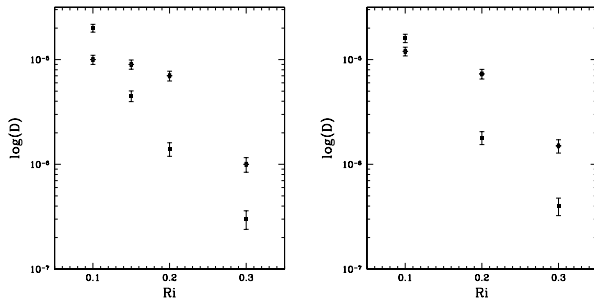


Figure 10. Dimensionless diffusion coefficient as a function of Richardson number for $B = 0.001$ (stars) and $B = 0.003$ (squares).

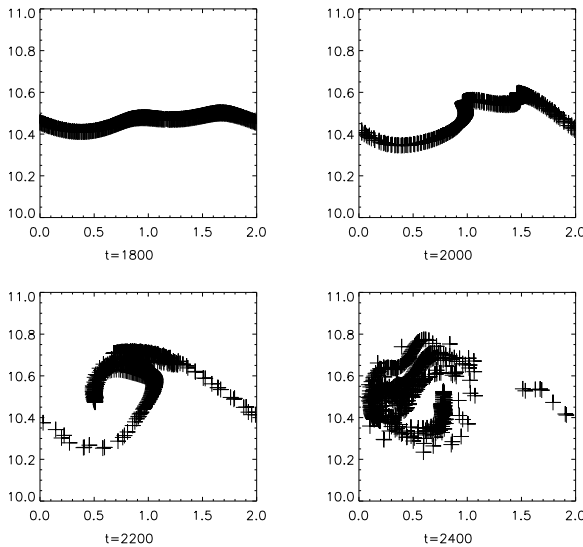


Figure 11. Positions of tracer particles at various times for a 3D simulation with $Ri=0.2$ and $B=0.001$.

press the formation of the vortex. In the simulations with higher Richardson numbers the 3D simulations yielded results more similar to the 2D simulations. This results agree with the findings of Ryu, Jones & Frank (2000) who also noted that in 3D the magnetic field is more disruptive than in 2D. However, for the case in which the magnetic field enhanced the mixing, i.e. with $B = 0.003$ and $Ri=0.1$, we found that the enhancement is somewhat less than the 2D simulations suggested.

This observation is fundamentally different from the simulations of the non-magnetic Kelvin-Helmholtz instability. In the non-magnetic case the differences between the mixing rates of the 2D and 3D simulations were not as strong. Now, with the inclusion of magnetic fields, the picture is different, and this constitutes one of the main results of this paper.

To investigate the origin of the discrepancy between the 2D and 3D simulations, we visualised the magnetic energy in isosurface plots. Figs. 13 shows that the magnetic field becomes very inhomogeneous and does not retain its symmetry in the y -direction. One can observe that the magnetic

field condenses into 6 - 8 flux tubes. In these flux tubes, the magnetic pressure is about 10 times as high as in the regions outside the flux tubes. This agrees with the simulations by Ryu, Jones and Frank (2000) who observe that the field becomes corrugated in the y -direction and then develops into flux tubes. These flux tubes are aligned with the flow and have the tendency to rise in the fluid due to their buoyancy. Flux tubes of the same polarity repel each other which explains their almost equidistant spacing in the horizontal which is seen in Fig. 13. This repulsion grows with the strength of the magnetic field. In our simulation we observed that the spacing between the flux tubes is bigger for higher magnetic field strengths. In the runs with a higher magnetic field fewer flux tubes formed. The lower flux tubes are observed to rise in the fluid and during this rise merge with neighbouring flux tubes. This transverse attraction of rising flux tubes is a well known phenomenon that has been observed, e.g., in the bipolar magnetic regions of the Sun. The attraction between rising flux tubes is caused by purely hydrodynamical forces (see, e.g. Parker 1979).

The flux tubes with their high field strengths become dynamically important. They induce vortical motions in the yz -plane which enhance the mixing rather than suppress it. In the run with $B = 0.001$ and $Ri=0.1$ we found that the magnetic field is enhanced even more than in the 2D simulations, namely by a factor of ~ 15 compared to ~ 12 in 2D. For runs with higher Richardson numbers the enhancement was similar or less than that found in the 2D simulations.

From the positions of the tracer particles we, again, calculate a diffusion coefficient. Its variation with the Richardson number is shown in Fig. 10. In general, the diffusion coefficient is higher than in the respective 2D case as discussed above. However, the behaviour is similar: D decreases with Ri and the magnetic field suppresses the mixing for all cases except for $Ri=0.1$.

We tested the robustness of our results by changing the size of the computational domain and the boundary conditions. We repeated some simulations with periodic boundary conditions in the y - direction and did not find any noteworthy differences to our results. The same was true for simulations on a grid that was twice as large in the z - direction. The nature of the boundaries changed the details of our results but did not change the global morphology of the flow.

3.3 Numerical viscosity

One frequently voiced objection to these kinds of direct numerical simulations is that Reynolds numbers as high as those encountered in most astrophysical conditions are unattainable on current computers, and that therefore the results are unrealistic. But, as pointed out by Balbus, Hawley & Stone (1996), this criticism is unjustified for simulations of the shear instability. They argue, that in order to simulate the onset of instability in a laminar flow, it is merely necessary that the ‘typical’ wavelength of the instability is resolved by the numerical scheme and that the numerical diffusion at this wavelength is less than the growth rate. This makes the simulation of shear instabilities an easier task than the simulation of viscous instabilities where in

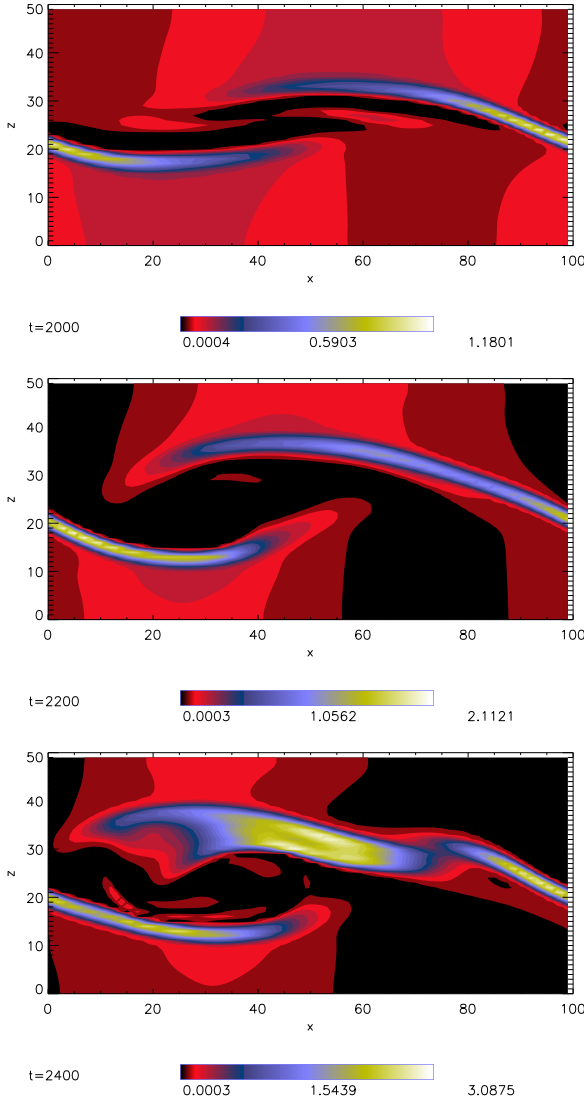


Figure 12. Magnetic energy in a slice along the xz -plane of a 3D simulation with $Ri=0.2$, $B = 0.001$.

theory one would have to resolve everything down to the viscous length scale.

Porter & Woodward (1994) have estimated the Reynolds number of hydrodynamical simulations based on a PPM (piecewise parabolic method) code. The Reynolds number depends on the truncation error of the finite-difference algorithm, the Courant number, the background advection and the number of grid points. They found that the effective Reynolds number is proportional to the third power of the number of grid points, with the main dissipation occurring at short wavelengths. Above this critical wavelength the diffusion was found to be small. Since the ZEUS code uses piecewise linear functions instead of piecewise parabolic functions, the truncation errors of ZEUS will be larger than those of a PPM code. But even if they were only proportional to the second power of the number of grid points in one direction, we would still expect a numerical

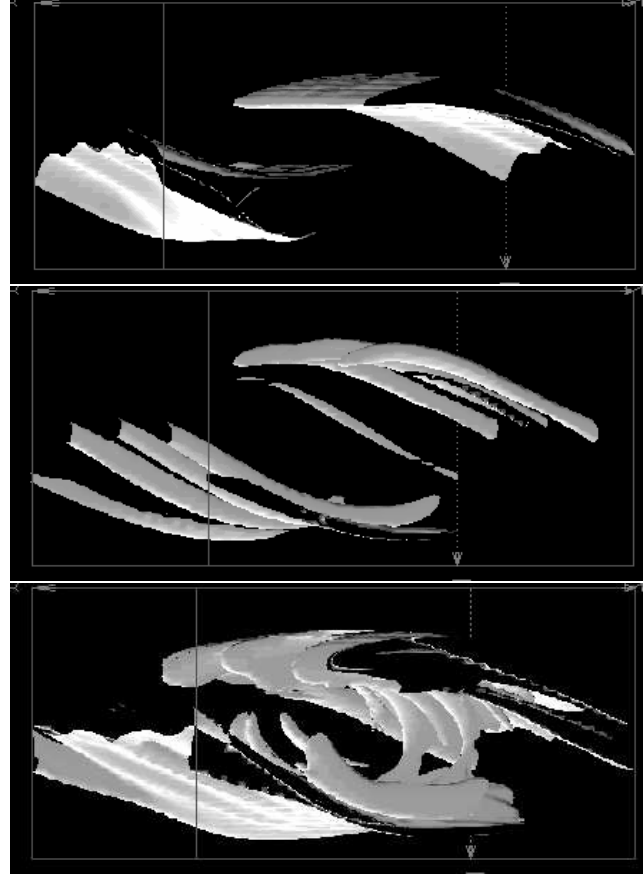


Figure 13. Magnetic energy in a 3D simulation with $Ri=0.1$, $B = 0.001$ at times $t = 2000$, $t = 2300$ and $t = 2500$.

Reynolds number of around 10^4 .

In ideal MHD simulations, numerical truncation errors also produce some numerical resistivity. Rough estimates based on the work of Ryu et al. (1995) suggest that the magnetic Reynolds number for our grid is < 100 .

If the flow is unbounded, there is no viscous boundary layer which might interfere with the results. The nonlinear instabilities are fundamentally inviscid in character. Therefore, for our purpose, we only need a resolution capable of resolving a range of wavelengths for which the numerical diffusion errors are less than the growth rates. Finally, we should emphasize that we are not claiming to have simulated magnetohydrodynamic turbulence. We merely simulated the Kelvin-Helmholtz instability and not full 3D turbulence which is a much more difficult problem and which requires a much finer (and yet unattained) numerical resolution.

4 CONCLUSIONS

In this paper we presented 2D and 3D simulations of the Kelvin-Helmholtz instability in magnetised and stratified shear flows.

We found that a uniform magnetic field parallel to the shear flow affects the evolution of the flow in a number of

ways. In most cases it suppresses the mixing as expected from linear stability analyses. However, for flows with low Richardson numbers and strong magnetic fields the evolution of the flow is strongly nonlinear and the magnetic field now enhances the mixing in the shear layer. The evolution of the magnetic shear instability is complex and rich: magnetic field lines stretch, bend and reconnect. Thereby, the magnetic field is locally enhanced. It forms flux tubes which, in turn, influence the dynamics of the flow as they merge and rise through the fluid.

For the cases in which the magnetic field suppresses shear instabilities, the 3D simulations reveal that a parallel magnetic field is less effective in suppressing the mixing than linear stability analyses and 2D simulations suggest. On the other hand, the field is less capable of enhancing the mixing for low Richardson numbers and strong magnetic fields as observed in 2D. The magnetic field concentrates in flux tubes which are dynamically important and enhance the mixing in the shear layer. This leads to motions in the plane transverse to the flow which further destabilise the flow. We investigated the mixing rate for a number of initial conditions that were characterised by the Richardson number and the magnetic field strength. Using tracer particles we quantified the mixing by a heuristic diffusion coefficient which is plotted in Fig. 10.

However, a direct application of our results, especially Fig. 10, should be treated with some caution. Our setup is rather artificial and was primarily intended to give some insights into the physics of the shear instability in magnetized flows. We have performed a parameter study on a rather restricted set of parameters, mostly because these simulations are computationally expensive. Further studies will have to extend, both, the number as well as the ranges of these parameters. The consequences of newly found diffusion coefficients on stellar evolution and elemental abundances, for example, are difficult to foresee. In stars, the speed as well as the depth of mixing determine the balance between mixing and nuclear burning. The effects of mixing will have to be studied in detail as they depend sensitively on the conditions prevailing in the star.

Finally, we should mention that a number of factors can inhibit or facilitate mixing such as gradients in the chemical potential of the fluid, diffusion of radiation and effects pertaining to the spherical geometry. In late-type stars strong chemical composition gradients exist, which will have a stabilising effect on the stratification. Therefore, especially for stellar evolution studies, the chemical composition gradient is an important parameter, which will have to be included in future work.

ACKNOWLEDGEMENTS

A part of the simulations were performed on computers of the Rechenzentrum Garching. We thank Phil Armitage and Henk Spruit for helpful discussions.

REFERENCES

Anzer, U., Börner, G., 1983, A&A, 122, 73
 Balbus, S.A., Hawley, J.F., & Stone, J.M., 1996, *Astrophys. J.*, 467, 76
 Brüggen, M., & Hillebrandt, W., 2000, MNRAS in press.
 Chandrasekhar, S., 1961, *Hydrodynamic and Hydromagnetic Stability*, Clarendon Press, Oxford
 Charbonnel, C., 1995, *Astrophys. J.*, 453, L41
 Denissenkov, P.A., 1994, A&A, 287, 113
 Denissenkov, P.A., & Tout, C.A., 2000, MNRAS in press
 Frank, A., Jones, T.W., Ryu, D., & Gaalaas, J.B., 1996, *Astrophys. J.* 460, 777
 Fransson, C. et al. 1989, *Astrophys. J.*, 336, 429
 Freytag, B., Ludwig, H.-G., Steffen, M. 1996, A&A, 313, 497
 Gough, D.O., & McIntyre, M.E., 1998, *Nature*, 394, 755
 Herrero, A. et al., 1992, A&A, 261, 209
 Jeong, H., Ryu, D., Jones, T.W., & Frank, A. 2000, *Astrophys. J.*, 529, 536
 Jones, T.W., Gaalaas, J.B., Ryu, D., & Frank, A., 1997, 482, 230
 Keppens, R., Tóth, G., Westermann, R.H.J., & Goedbloed, J.P., 1999, *J. Plasma Phys.*, 61, 1
 Kraft, R.P., 1994, PASP, 106, 553
 Kraft, R.P., Sneden, C., Smith, G.H., Shetrone, M.D., Langer, G.E., Pilachowski, C.A., 1997, AJ 113, 279
 Langer, N., 1992, A&A, 265, L17
 Langer, N., Maeder, A., 1995, A&A, 295, 685.
 Maeder, A., 1997, A&A, 321, 134
 Maeder, A., 1995, A&A, 299, 84
 Maeder, A., Zahn, J.-P., 1998, A&A, 334, 1000
 Malagoli, A., Bodo, G., & Rosner, R., 1996, ApJ, 456, 708
 Meynet, G., & Maeder, A., 1997, A&A, 321, 465
 Miura, A., & Pritchett, P.L., 1982, *J. Geophys. Res.*, 87, 7431
 Nordlund, A., Stein, R.F. 1996
 Parker, E.N., 1979, *Cosmical Magnetic Fields*, Clarendon, Oxford
 Porter, D.H., & Woodward, P.R., 1994, ApJS, 93, 309
 Ryu, D., Jones, T.W., & Frank, A., 2000, ApJ, in press.
 Singh, H. P., Roxburgh, I. W., Chan, K. L. 1998, A&A, 340, 178
 Spiegel, E.A., & Zahn, J.-P., 1992, A&A, 265, 106
 Stone, J.M., & Norman, M.L., 1992a, ApJS, 80, 753
 Stone, J.M., & Norman, M.L., 1992b, ApJS, 80, 791
 Uberoi, C., 1984, *J. Geophys. Res.*, 89, 5652
 Venn, K.A., Lambert, D.L. & Lemke, M. 1996, A&A, 307, 894
 Vietri, M., Ferrara, A., & Miniati, F., 1997, ApJ, 483, 262.
 Zahn, J.-P. 1991, A&A, 252, 179